Large Orbital Moment and Dynamical Jahn-Teller Effect of AlCl-Phthalocyanine on Cu(100)

Chao Li,[1] Marie-Laure Bocquet,[2] Yan Lu,[3] Nicolas Lorente,[4,5] Manuel Gruber,[1,6] Richard Berndt,[1] and Alexander Weismann[1,*]

[1]*Institut für Experimentelle und Angewandte Physik, Christian-Albrechts-Universität zu Kiel, D-24098 Kiel, Germany*
[2]*Laboratoire de physique de l école normale supérieure, ENS, Université PSL, CNRS, Sorbonne Université, Université Paris Cité, Paris, France*
[3]*Department of Physics, Nanchang University, Nanchang 330031, People's Republic of China*
[4]*Centro de Física de Materiales CFM/MPC (CSIC-UPV/EHU), E-20018 Donostia-Sebastián, Spain*
[5]*Donostia International Physics Center (DIPC), E-20018 Donostia-Sebastián, Spain*
[6]*Faculty of Physics and CENIDE, University of Duisburg-Essen, 47057 Duisburg, Germany*

(Received 17 July 2023; revised 3 April 2024; accepted 15 August 2024; published 18 September 2024)

Submonolayer amounts of chloroaluminum-phthalocyanine on Cu(100) were studied with scanning tunneling spectroscopy. The molecule can be prepared in a fourfold symmetric state whose conductance spectrum exhibits a zero-bias feature similar to a Kondo resonance. In magnetic fields, however, this resonance splits far more than expected from the spin of a single electron. Density functional theory calculations reveal a charge transfer of 1.3 electrons to the degenerate lowest unoccupied molecular orbitals. These orbitals are mixed by the orbital momentum operator $\hat{L}_z$ with a large matrix element corresponding to $m_L \approx 2.7$. Dehydrogenation of a ligand lifts the degerenracy of the lowest unoccupied molecular orbital, reduces the splitting in magnetic fields, and induces a polarity dependence of the spectra. Using model calculations of the spin, orbital, and vibrational degrees of freedom we show that a dynamical Jahn-Teller effect reproduces the main experimental observations.

DOI: 10.1103/PhysRevLett.133.126201

Applications of magnetic molecules as building blocks in data storage and quantum information technology could benefit from the reliability and purity of chemical syntheses and the high degree of order that may be achieved by molecular self-assembly [1–3]. Molecular constituents can in principle be designed to control the size of a local magnetic moment, the magnetic anisotropy, and the coupling to substrate electrons [4,5]. Transition metal ions are usually employed to obtain a magnetic moment and multiple ions are combined in correspondingly complex molecules to achieve large moments [6,7]. Although the orbital magnetic moment is crucial for reaching large spin anisotropy via spin-orbit interaction [8,9], angular momentum is usually not considered in molecular systems because it is not a good quantum number when rotational invariance is lacking.

Here, we present results for the diamagnetic fourfold symmetric molecule chloroaluminum-phthalocyanine (ClAlPc) [Fig. 1(a)] that surprisingly acquires a large orbital magnetic moment on Cu(100) by charge transfer. The molecule has two degenerate lowest unoccupied molecular orbitals (LUMOs) that are partially occupied. We show that these orbitals combine to left and right circulating states with large angular momentum.

Experiments were performed with a low temperature scanning tunneling microscope (STM, UNISOKU USM-1300) at sample temperatures of 0.34 and 4 K and in magnetic fields of up to 9 T perpendicular to the sample surface. Cu(100) single crystals were prepared by Ar^+ sputtering and annealing. ClAlPc molecules were deposited from a Knudsen cell onto the Cu surface held at room temperature. STM tips were electrochemically etched from W wire and sputtered in ultrahigh vacuum. For spectroscopy of the differential conductance dI/dV, current feedback was disabled at 50 mV and 500 pA and a sinusoidal modulation of 0.5 mV_{pp} with 831 Hz was added to the sample voltage V.

Similar to previous studies of ClAlPc [10–15], STM topographs reveal two distinct fourfold symmetric patterns of the molecules on Cu(100) [Fig. 1(c)] that we attribute to adsorption geometries with the Cl ion either pointing away from (Cl-up) or toward (Cl-dn) the substrate [Fig. 1(b)]. Cl-dn molecules can be converted to a new state R by placing the tip above the molecule and raising V above 2.5 V [Fig. 1(d)] until the tunneling current suddenly drops. R appears as an approximately ring-shaped protrusion while preserving C_4 symmetry. Similar to other phthalocyanines [16,17], the STM patterns of ClAlPc are chiral

*Contact author: weismann@physik.uni-kiel.de

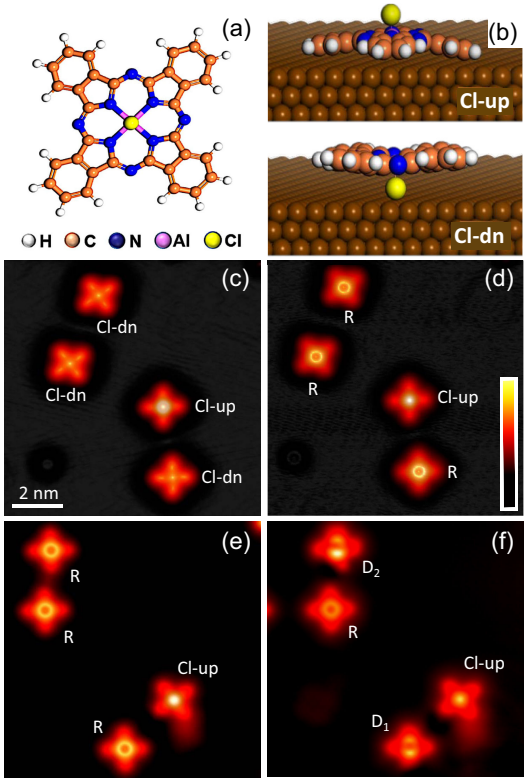

FIG. 1. (a) Scheme of ClAlPc and (b) its adsorption geometries Cl-up (top) and Cl-dn (bottom) on Cu(100). (c) STM topograph of deposited ClAlPc. (d) Same area after converting three Cl-dn molecules to new state R. (e) and (f) R molecules transformed further to states D_1 and D_2 by voltage pulses. Imaging parameters: $I = 100$ pA; $V = 0.5$ V in (c), 0.1 V in (d)–(f). The false color scheme used is displayed in (d) and covers height ranges of 210 and 230 pm in (c)–(e) and (f), respectively.

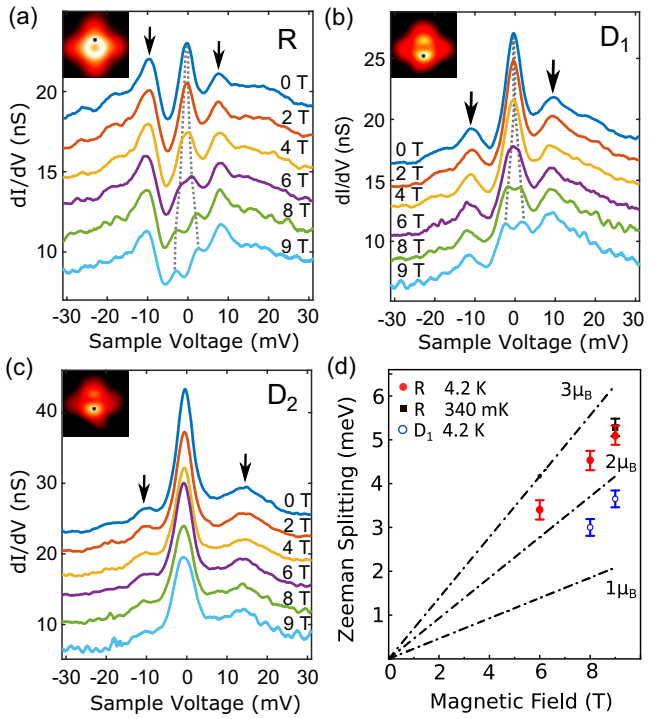

FIG. 2. dI/dV spectra of states (a) R, (b) D_1, and (c) D_2 measured in magnetic fields at $T = 4$ K. Arrows indicate reproducible satellite peaks. Insets show topographs with the positions used for spectroscopy marked by dots. Parameters used before opening the feedback loop: $V = 50$ mV, $I = 500$ pA. The spectra in a and b (c) were shifted upward in increments of 2 (3.5) nS for clarity, with no shift applied to the 9 T data. (d) Splitting of the zero-bias peak vs magnetic field for R (red dots and black square) and D_1 (blue circles). Lines show the splitting expected for magnetic moments of 1, 2, and 3 μ_B.

with its isoindole lobes oriented at $\approx \pm 27°$ relative to a substrate $\langle 110 \rangle$ direction. As shown in the Supplemental Material [18] conversion was reversible at elevated temperatures ($T = 18$ K), demonstrating that R and Cl-dn are identical molecules.

Further voltage pulses applied above the molecular lobes reduce the symmetry to approximately C_2 [Figs. 1(e) and 1(f)] presumably via dehydrogenation as reported in Refs. [23] and [24]. A dumbbell pattern is observed at small positive V while the patterns at low negative V are similar to R. We denote these molecules D_1 (D_2) after one (two) dehydrogenation processes of a single lobe.

Figure 2(a) shows dI/dV spectra of R molecules. A sharp resonance is resolved around zero bias along with satellite peaks at $V \approx \pm 10$ mV, similar to those in Ref. [25]. The peaks are strongest above the ring-shaped protrusion and weaker above the molecular center. The spectra of dehydrogenated molecules [D_1, D_2, Figs. 2(b) and 2(c)] are qualitatively similar but the amplitude of the zero-bias peak increases from R over D_1 to D_2.

Density-functional theory calculations reproduce the distinct states R and Cl-dn. Depending on the starting geometry used, the structure optimization converged to states with different geometries and magnetic moments. One of them is nonmagnetic with the isoindole lobes oriented at $\approx \pm 26°$ relative to a substrate $\langle 110 \rangle$ direction. We assign it to Cl-dn. The second metastable geometry has a slightly different orientation ($\approx \pm 24°$), is paramagnetic, and the vertical atom positions differ from those of Cl-dn by up to 15 pm. In this state, the LUMO is occupied by 1.3 electrons and it is spin-polarized. This is consistent with the experimental state R. Calculations for intermediate geometries (Supplemental Material [18]) revealed an energy barrier of ≈20 meV between the metastable states. Adsorption induced magnetic bistability was previously reported from hexaazatriphenylenehexacarbonitrile on Ag(111) [26].

Next we apply magnetic fields B perpendicular to the surface to reveal a magnetic origin of the zero-bias resonance. For R, the field splits the peak and reduces its amplitude [Fig. 2(a)]. The splitting is smaller for D_1 [Fig. 2(b)] and not discernible for D_2 [Fig. 2(c)], where an amplitude reduction and some broadening occur. Additional 340 mK data are available for 0 and 9 T

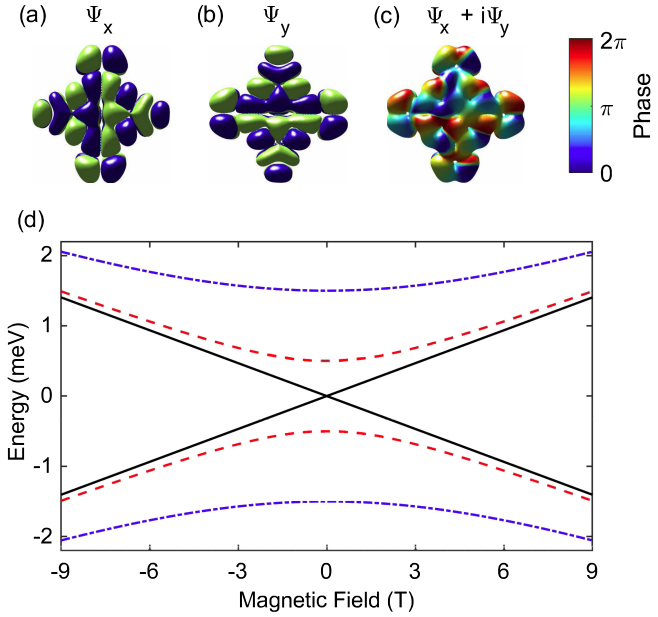

FIG. 3. Pseudoilluminated surfaces of constant electron density of the ClAlPc LUMOs (a) Ψ_x and (b) Ψ_y from density-functional theory calculations. Colors show the phase of the wave functions. The Cl atom is located behind the molecular plane. (c) A superposition state $(\Psi_x + i\Psi_y)/\sqrt{2}$ with an orbital moment of $2.7\,\mu_B$. (d) Orbital Zeeman splitting of linear combinations of statesΨ_x and Ψ_y with matrix element $|\langle\Psi_x|L_z|\Psi_y\rangle| = 2.7\hbar$. The black curve corresponds to orbital degeneracy ($\varepsilon_x = \varepsilon_y$). Red dashed and blue dash-dotted lines show results for static LUMO splittings $|\varepsilon_x - \varepsilon_y|$ of 1 and 3 meV, respectively. Splitting is expected to occur when the symmetry of the molecule is lowered by dehydrogenation of one of the isoindole subunits.

(Supplemental Material [18]) and exhibit sharper lines with identical splitting. Figure 2(d) shows the peak positions. Assuming a linear Zeeman splitting, magnetic moments of 2.5 and $1.8\,\mu_B$ are extracted for R and D_1, respectively. These values are surprisingly large: the largest possible spin moment of $2\,\mu_B$ ($S = 1$) requires a charge transfer of two electrons with parallel spins to the originally diamagnetic molecule [27].

Since spin is an unlikely source of the large magnetic moment, we now consider angular momentum. The calculated degenerate LUMOs Ψ_x and Ψ_y are C_2-symmetric [Figs. 3(a),(b)] and have zero L_z-expectation value. However, left and right circulating superposition states $\Psi_\pm = (\Psi_x \pm i\Psi_y)/\sqrt{2}$ [Fig. 3(c)] exhibit an astonishingly large $m_L = |\langle\Psi_\pm|L_z|\Psi_\pm\rangle/|\hbar = 2.7$.

Although a 180° rotation inverts the sign of both LUMOs similar to atomic p orbitals with $L = 1$, the phase along the inner macrocycle undergoes five oscillations per revolution, which would imply $L = 5$ in the case of an electron on a ring. However, the Pc macrocycle is not perfectly circular and in addition the LUMO density extends beyond the macrocycle. Together, these factors reduce the orbital moment to $m_L = 2.7$. This mutual interlocking of degenerate wave functions is also the source of molecular ring currents in other macrocyclic molecules [30–32]. Below we show that this is the main reason for the large observed magnetic moment.

Open-shell molecules with degenerate ground states are prone to Jahn-Teller (JT) instability, which lowers the total energy by a distortion, lifts orbital degeneracy [33], and may quench the orbital moment. The quenching depends on the energy $m_L\mu_B B$ compared to the zero-field splitting of the LUMOs, $\Delta\varepsilon = |\varepsilon_x - \varepsilon_y|$. As an example, Fig. 3(d) shows the Zeeman splitting of two states at ε_x and $\varepsilon_y = \varepsilon_x + \Delta\varepsilon$ that are mixed via $\pm i m_L\mu_B B$ using $m_L = 2.7$. For $B \leq 9$ T, the splitting reduces the slope dE/dB significantly below $m_L\mu_B$, the value found for $\varepsilon_x = \varepsilon_y$. However, the present system is more complex. The molecule and the substrate are C_4 symmetric and consequently a second JT-distorted state, whose displacement pattern is rotated by 90°, has the same total energy and inverted splitting, $\varepsilon_y = \varepsilon_x - \Delta\varepsilon$. Transitions between these two ground states, coupled with dynamic fluctuations in the JT distortion and orbital occupation resulting in the emergence of the Kondo effect, are expected to give rise to a zero-bias resonance in dI/dV, as has been experimentally observed.

To test the impact of such a dynamical JT effect on the orbital moment, we simulated experimental dI/dV spectra by extending the spin model of Ref. [29] to include orbital and vibrational degrees of freedom. The electron subsystem is modeled by two LUMOs Ψ_x and Ψ_y, which each may be occupied by electrons of arbitrary spin ($\sigma = \uparrow, \downarrow$) and a Coulomb repulsion U controlling the total occupation. A magnetic field B oriented in z direction splits $\uparrow$ and $\downarrow$ states via the Zeeman term, mixes the LUMOs via $\pm i m_L\mu_B B$, and splits left and right circulating states $\psi_\pm$. The JT distortion is modeled by a single vibration mode whose harmonic oscillator potential is shifted along its normal coordinate by $d(n_x - n_y)$, where n_x (n_y) are the occupation numbers of Ψ_x (Ψ_y) and d is a constant. The same coupling also splits the LUMOs when the molecule is distorted. Details of the calculations and additional results may be found in the Supplemental Material [18]. Below we summarize important findings.

The model predicts complex spectra because both spin and orbital excitation steps are present and merge when the effective temperature is raised. Figure 4(a) shows results for the C_4 symmetric case ($\varepsilon_x = \varepsilon_y$) at $T = 4$ K. At $B = 0$, four degenerate ground states exist that differ in spin and orbital occupation numbers (n_x,n_y) with concomitant JT distortions. The calculated spectra at 0 T (upper curve) show a zero-bias resonance and satellite peaks on either side, each separated by the vibration energy $\hbar\omega$ when JT coupling is included. A magnetic field (lower curve) splits the central resonance and reduces its amplitude. The model thus qualitatively reproduces the experimental data of

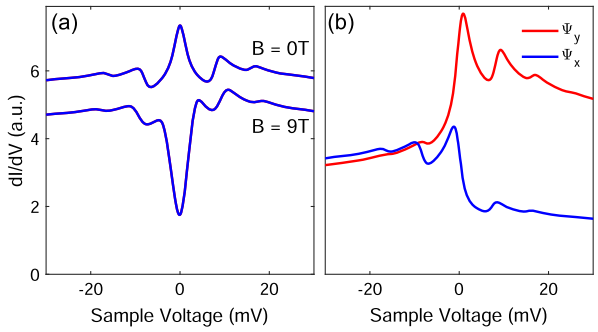

FIG. 4. Spin-averaged conductance spectra calculated for $T = 4$ K assuming one relevant JT mode at $\hbar\omega = 8$ meV and $d = 0.5D$, where D is the characteristic length of the harmonic oscillator potential (see Fig. S11 in the Supplemental Material). (a) C_4 symmetric case for $B = 0$ (upper curve, vertically offset by 1 a.u.) and 9 T (lower curve). (b) C_2 symmetric case using an energy splitting between Ψ_x and Ψ_y of 0.4 meV. Ψ_x (blue) and Ψ_y (red) exhibit different spectra at $V > 0$ but match at negative bias.

Fig. 2(a). The value $m_L = 2.7$ obtained from the gas-phase wave functions leads to a larger splitting than experimentally observed. The LUMO of the adsorbed molecule, however, partially delocalizes into the substrate and a reduction of m_L is consequently expected.

Figures 5(a) and (b) display topographs of the C_2-symmetric state D_1. Data for state D_2 may be found in the Supplemental Material [18]. The corresponding dI/dV spectra [Figs. 5(c) and S3] depend on the lateral position of the STM tip. In particular, the zero-bias resonances of both states are drastically stronger on the lobe that appears highest in topographs measured at $V > 0$. The central peak of D_2 is larger and all features are broader than for D_1.

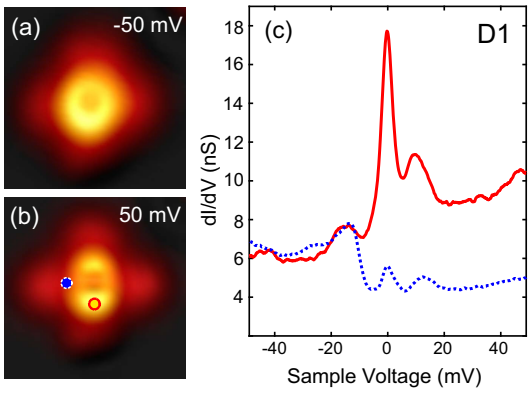

FIG. 5. Position dependence of inelastic signatures. (a) and (b) show topographs of D_1 measured at 100 pA and ± 50 mV. The color scale covers ranges of 190 and 210 pm, respectively. (c) dI/dV spectra. The red solid (blue dotted) line corresponds to the position marked in (b) with a red circle (blue dot). Parameters used before disabling feedback: 50 mV, 500 pA. The dotted curve has been scaled by 0.48 to approximately match the tip height used for measuring the solid line.

Importantly, the intensity ratio of the satellites at negative and positive bias is inverted between orthogonal lobes of the molecule (Fig. 5, red and blue markers). This is reproduced by the model when ε_x and ε_y differ by small values in the 100 μeV range. Ψ_x and Ψ_y are then differently occupied. As a result, inelastic orbital excitations can be induced by adding an electron to the empty orbital ($V > 0$) or removing an electron from the filled orbital ($V < 0$).

The calculated conductances of both orbitals are similar for $V < 0$ and strongly deviate at $V > 0$ [Fig. 4(b)]. These differences are due to inelastic processes, which dominate the tunneling current close to zero bias. Consequently, the deviations between topographs of D_1 and D_2 at different polarities are caused by inelastic current contributions.

An explanation of inelastic satellites via a static Jahn-Teller effect has been discussed in Ref. [34]. In such a scenario, orbital-flip processes lead to inelastic features at voltages corresponding to the LUMO splitting. In our experimental data, however, satellites at almost identical energies are also present for state R, where no splitting between the LUMOs is expected because of the C_4 symmetry. We therefore exclude that the energy of the satellite peaks corresponds to the LUMO splitting. Rather it reflects the vibrational energy $\hbar\omega$.

Some limitations of our model should be mentioned. First, perturbation theory does not correctly predict the amplitude, width, and shape of Kondo resonances [29], except for a weak-coupling regime [35]. As elastic orbital-flip excitations can also be mediated by substrate electrons, the system dynamically fluctuates between both degenerate JT distortions, and a correlated superposition is likely to occur. This is analogous to a Kondo effect, where dynamical spin fluctuations due to exchange scattering with substrate electrons produce a singlet ground state for which the Kondo resonance retains a finite width and amplitude even at $T = 0$, unlike the zero-bias resonance from perturbation theory. The model therefore cannot reproduce the evolution of the amplitudes and widths of the zero-bias resonance from R via D_1 to D_2. Second, only a single vibration is considered while Jahn-Teller distortion involves multiple modes with different frequencies that are expected to broaden the satellites, especially those of higher order [36].

In summary, magnetic fields split the zero-bias resonance in the conductance spectra of ClAlPc on Cu(100) much more than expected. This effect is due to a large orbital moment, which is not suppressed by a static Jahn-Teller distortion. Rather, the ground state dynamically fluctuates between two distorted molecular configurations. When the molecular C_4 symmetry is broken by dehydrogenation the orbital moment is reduced, and inelastic contributions to the tunneling exhibit a strong asymmetry

with respect to bias polarity and tip position. Related observations are expected for other molecules with partially occupied degenerate ground states and suitable wave functions.

Acknowledgments—M. G. acknowledges funding from the Deutsche Forschungsgemeinschaft (DFG, German Research Foundation) Project No. 278162697-SFB 1242.

[1] L. Bogani and W. Wernsdorfer, Molecular spintronics using single-molecule magnets, Nat. Mater. **7**, 179 (2008).
[2] M. Holynska, *Single-Molecule Magnets Molecular Architectures and Building Blocks for Spintronics* (John Wiley & Sons, Limited, New York, 2018), p. 456.
[3] A. Gaita-Ariño, F. Luis, S. Hill, and E. Coronado, Molecular spins for quantum computation, Nat. Chem. **11**, 301 (2019).
[4] C. J. Milios, A. Vinslava, W. Wernsdorfer, S. Moggach, S. Parsons, S. P. Perlepes, G. Christou, and E. K. Brechin, A record anisotropy barrier for a single-molecule magnet, J. Am. Chem. Soc. **129**, 2754 (2007).
[5] E. Coronado, Molecular magnetism: From chemical design to spin control in molecules, materials and devices, Nat. Rev. Mater. **5**, 87 (2019).
[6] S. Kahle, Z. Deng, N. Malinowski, C. Tonnoir, A. Forment-Aliaga, N. Thontasen, G. Rinke, D. Le, V. Turkowski, T. S. Rahman, S. Rauschenbach, M. Ternes, and K. Kern, The quantum magnetism of individual manganese-12-acetate molecular magnets anchored at surfaces, Nano Lett. **12**, 518 (2011).
[7] J. A. Burgess, L. Malavolti, V. Lanzilotto, M. Mannini, S. Yan, S. Ninova, F. Totti, S. Rolf-Pissarczyk, A. Cornia, R. Sessoli, and S. Loth, Magnetic fingerprint of individual Fe_4 molecular magnets under compression by a scanning tunnelling microscope, Nat. Commun. **6**, 8216 (2015).
[8] L. Sorace, C. Benelli, and D. Gatteschi, Lanthanides in molecular magnetism: Old tools in a new field, Chem. Soc. Rev. **40**, 3092 (2011).
[9] I. G. Rau, S. Baumann, S. Rusponi, F. Donati, S. Stepanow, L. Gragnaniello, J. Dreiser, C. Piamonteze, F. Nolting, S. Gangopadhyay, O. R. Albertini, R. M. Macfarlane, C. P. Lutz, B. A. Jones, P. Gambardella, A. J. Heinrich, and H. Brune, Reaching the magnetic anisotropy limit of a 3*d* metal atom, Science **344**, 988 (2014).
[10] Y. L. Huang, R. Wang, T. C. Niu, S. Kera, N. Ueno, J. Pflaum, A. T. S. Wee, and W. Chen, One dimensional molecular dipole chain arrays on graphite via nanoscale phase separation, Chem. Commun. (Cambridge) **46**, 9040 (2010).
[11] Y. L. Huang, Y. Lu, T. C. Niu, H. Huang, S. Kera, N. Ueno, A. T. S. Wee, and W. Chen, Reversible single-molecule switching in an ordered monolayer molecular dipole array, Small **8**, 1423 (2012).
[12] Y. L. Huang, W. Chen, F. Bussolotti, T. C. Niu, A. T. S. Wee, N. Ueno, and S. Kera, Impact of molecule-dipole orientation on energy level alignment at the submolecular scale, Phys. Rev. B **87**, 085205 (2013).
[13] T. Niu, M. Zhou, J. Zhang, Y. Feng, and W. Chen, Dipole orientation dependent symmetry reduction of chloroaluminum phthalocyanine on Cu(111), J. Phys. Chem. C **117**, 1013 (2013).
[14] H. Song, C. Fu, N. Li, H. Zhu, Z. Peng, W. Zhao, J. Dai, L. Xing, Z. Huang, W. Chen, Y. Wang, J. Yang, and K. Wu, On the shuttling mechanism of a chlorine atom in a chloroaluminum phthalocyanine based molecular switch, Phys. Chem. Chem. Phys. **19**, 22401 (2017).
[15] M. D. Jiménez-Sánchez, N. Sánchez-Abad, N. Nicoara, and J. M. Gómez-Rodríguez, Self-assembly of ClAlPc molecules on moiré-patterned graphene grown on Pt(111), Surf. Sci. **710**, 121848 (2021).
[16] A. Mugarza, N. Lorente, P. Ordejón, C. Krull, S. Stepanow, M.-L. Bocquet, J. Fraxedas, G. Ceballos, and P. Gambardella, Orbital specific chirality and homochiral self-assembly of achiral molecules induced by charge transfer and spontaneous symmetry breaking, Phys. Rev. Lett. **105**, 115702 (2010).
[17] A. Mugarza, R. Robles, C. Krull, R. Korytár, N. Lorente, and P. Gambardella, Electronic and magnetic properties of molecule-metal interfaces: Transition-metal phthalocyanines adsorbed on Ag(100), Phys. Rev. B **85**, 155437 (2012).
[18] See Supplemental Material, which includes Refs. [19–22], at http://link.aps.org/supplemental/10.1103/PhysRevLett.133.126201 for additional experimental data, density-functional theory results, and model calculations.
[19] J. P. Perdew, K. Burke, and M. Ernzerhof, Generalized gradient approximation made simple, Phys. Rev. Lett. **77**, 3865 (1996).
[20] S. Grimme, J. Antony, S. Ehrlich, and H. Krieg, A consistent and accurate *ab initio* parametrization of density functional dispersion correction (DFT-D) for the 94 elements H-Pu, J. Chem. Phys. **132**, 154104 (2010).
[21] J. R. Schrieffer and P. A. Wolff, Relation between the Anderson and Kondo Hamiltonians, Phys. Rev. **149**, 491 (1966).
[22] C. Rubio-Verdú, A. Sarasola, D.-J. Choi, Z. Majzik, R. Ebeling, M. R. Calvo, M. M. Ugeda, A. Garcia-Lekue, D. Sánchez-Portal, and J. I. Pascual, Orbital-selective spin excitation of a magnetic porphyrin, Commun. Phys. **1**, 15 (2018).
[23] Y. F. Wang, J. Kröger, R. Berndt, H. Vázquez, M. Brandbyge, and M. Paulsson, Atomic-scale control of electron transport through single molecules, Phys. Rev. Lett. **104**, 176802 (2010).
[24] A. Zhao, Q. Li, L. Chen, H. Xiang, W. Wang, S. Pan, B. Wang, X. Xiao, J. Yang, J. G. Hou, and Q. Zhu, Controlling the Kondo effect of an adsorbed magnetic ion through its chemical bonding, Science **309**, 1542 (2005).
[25] D. Rakhmilevitch, R. Korytár, A. Bagrets, F. Evers, and O. Tal, Electron-vibration interaction in the presence of a switchable Kondo resonance realized in a molecular junction, Phys. Rev. Lett. **113**, 236603 (2014).
[26] A. Chakraborty, P. Zahl, Q. Dai, H. Li, T. Fritz, P. Simon, J.-L. Brédas, and O. L. A. Monti, Frontier orbital degeneracy: A new concept for tailoring the magnetic state in organic semiconductor adsorbates, J. Phys. Chem. C **127**, 23504 (2023).

[27] The field dependence of the peak energies may deviate to lower values for a spin-split Kondo resonance [28]. This would imply an underestimation of the magnetic moment and make the determined moments even more surprising. Third-order perturbation theory, on the other hand, predicts that the spectral maxima caused by inelastic tunneling can be shifted above the excitation energy when temperature broadening is taken into account [29]. While this could lead to an exaggerated magnetic moment, in the present case, the splitting is independent of temperature (4.2 and 0.34 K) ruling out this possibility.

[28] T. A. Costi, Kondo effect in a magnetic field and the magnetoresistivity of Kondo alloys, Phys. Rev. Lett. **85**, 1504 (2000).

[29] M. Ternes, Spin excitations and correlations in scanning tunneling spectroscopy, New J. Phys. **17**, 063016 (2015).

[30] F. London, Théorie quantique des courants interatomiques dans les combinaisons aromatiques, J. Phys. Radium **8**, 397 (1937).

[31] M. Jirásek, H. L. Anderson, and M. D. Peeks, From macrocycles to quantum rings: Does aromaticity have a size limit?, Acc. Chem. Res. **54**, 3241 (2021).

[32] A. Kaito, A. Tajiri, and M. Hatano, Calculations of the magnetic moments of some benzene derivatives, J. Am. Chem. Soc. **97**, 5059 (1975).

[33] A. V. Kuzmin, S. S. Khasanov, K. P. Meletov, and R. P. Shibaeva, Jahn-Teller distortions of metal phthalocyanine anions $[M^{IV}OPc]^{n-}$ (M = Ti, V), J. Exp. Theor. Phys. **128**, 878 (2019).

[34] J. Kügel, P.-J. Hsu, M. Böhme, K. Schneider, J. Senkpiel, D. Serrate, M. Bode, and N. Lorente, Jahn-Teller splitting in single adsorbed molecules revealed by isospin-flip excitations, Phys. Rev. Lett. **121**, 226402 (2018).

[35] Y. hui Zhang, S. Kahle, T. Herden, C. Stroh, M. Mayor, U. Schlickum, M. Ternes, P. Wahl, and K. Kern, Temperature and magnetic field dependence of a Kondo system in the weak coupling regime, Nat. Commun. **4**, 2110 (2013).

[36] F. Schwarz, Y. F. Wang, W. A. Hofer, R. Berndt, E. Runge, and J. Kröger, Electronic and vibrational states of single tin-phthalocyanine molecules in double layers on Ag(111), J. Phys. Chem. C, 15716 (2015).